4D volcano gravimetry

Maurizio Battaglia[1,2], Joachim Gottsmann[3], Daniele Carbone[4], and José Fernández[5]

ABSTRACT

Time-dependent gravimetric measurements can detect subsurface processes long before magma flow leads to earthquakes or other eruption precursors. The ability of gravity measurements to detect subsurface mass flow is greatly enhanced if gravity measurements are analyzed and modeled with ground-deformation data. Obtaining the maximum information from microgravity studies requires careful evaluation of the layout of network benchmarks, the gravity environmental signal, and the coupling between gravity changes and crustal deformation. When changes in the system under study are fast (hours to weeks), as in hydrothermal systems and restless volcanoes, continuous gravity observations at selected sites can help to capture many details of the dynamics of the intrusive sources. Despite the instrumental effects, mainly caused by atmospheric temperature, results from monitoring at Mt. Etna volcano show that continuous measurements are a powerful tool for monitoring and studying volcanoes.

Several analytical and numerical mathematical models can beused to fit gravity and deformation data. Analytical models offer a closed-form description of the volcanic source. In principle, this allows one to readily infer the relative importance of the source parameters. In active volcanic sites such as Long Valley caldera (California, U.S.A.) and Campi Flegrei (Italy), careful use of analytical models and high-quality data sets has produced good results. However, the simplifications that make analytical models tractable might result in misleading volcanological interpretations, particularly when the real crust surrounding the source is far from the homogeneous/isotropic assumption. Using numerical models allows consideration of more realistic descriptions of the sources and of the crust where they are located (e.g., vertical and lateral mechanical discontinuities, complex source geometries, and topography). Applications at Teide volcano (Tenerife) and Campi Flegrei demonstrate the importance of this more realistic description in gravity calculations.

INTRODUCTION

Whether volcanic eruptions are the result of single intrusions or are the culmination of multiple intrusions that supply a reservoir, multiparameter monitoring techniques and robust mathematical models are essential for providing effective warnings to civil authorities and the public. Gravity measurements are an indispensable component for any volcano monitoring strategy and are the focus in this paper. A key assumption behind gravity monitoring is that changes in earth's gravity reflect mass-transport processes at depth (Dzurisin, 2003). However, because of the complexity of subsurface structures beneath active volcanoes, identifying the source of unrest is not straightforward. Active volcanoes often host both hydrothermal and magmatic reservoirs at depth. Physical and chemical changes in either can produce measurable geophysical signals. The challenge is to interpret these signals and infer the cause of unrest before impending eruptions (Johnsen et al., 1980; Dvorak and Dzurisin, 1997).

The intrinsic ambiguity in interpretation of gravity and/or geodetic data alone can be partially removed if they are analyzed jointly. Various authors have shown that combined time-dependent geodetic and gravimetric measurements are a key tool for mid- to long-term hazard assessment because they enable detection of subsurface mass redistribution long before other eruption precursors appear. (See examples in Dzurisin, 2003; Rymer and Williams-Jones, 2000; Gottsmann and Rymer, 2002; Sparks, 2003; and Battaglia et al., 2006.)

[1]U. S. Geological Survey, Volcano Hazards Team, Menlo Park, California, U.S.A
[2]University of Rome "La Sapienza," Department of Earth Sciences, Rome, Italy. E-mail: maurizio.battaglia@uniroma1.it.
[3]Department of Earth Sciences, University of Bristol, United Kingdom. E-mail: j.gottsmann@bristol.ac.uk.
[4]Istituto Nazionale di Geofisica e Vulcanologia, Sezione di Catania, Catania, Italy. E-mail: carbone@ct.ingv.it.
[5]Instituto de Astronomía y Geodesia (CSIC-UCM), Madrid, Spain. E-mail: jose_fernandez@mat.ucm.es

The critical questions that emerge when monitoring volcanoes are how to constrain the source of unrest, how to better assess hazards associated with the unrest, and how to refine our ability to forecast volcanic activity. Note that ground-deformation data alone cannot discriminate between magma and aqueous-fluid intrusion. Deformation measurements are sensitive to changes in the source pressure or volume only. They are completely independent from the nature of the source. This ambiguity can be resolved if we know the density of the source. Gravity measurements, however, can constrain the mass of the intrusion. Combined geodesy and gravity measurements can be used to infer the density of the intrusive fluids and can better constrain the source of unrest (Battaglia et al., 2006; Gottsmann et al., 2006a).

For volcano monitoring and risk mitigation, assessing gravity time changes is especially important when they occur without measurable ground deformation (Rymer et al., 1993; Carbone et al., 2003a; Gottsmann et al., 2006b).

In this paper, we review the state of the art of identifying sources of volcano unrest using microgravity studies. In particular, we discuss the potential and the challenges of repeated and continuous gravity measurements as tools for monitoring and studying active volcanoes. We also review the analytical and numerical mathematical models available in the literature that can be used to fit and interpret the observations.

FIELD SETUP AND SURVEY DESIGN

In designing a survey network at a volcano, it is important to bear in mind the signal from individual sources. Mass/pressure variations in at least three different levels of subsurface reservoirs might produce observable gravimetric signals at the ground surface:

1) Hydrothermal reservoirs, extending from surface levels to a few kilometers deep
2) Midcrustal reservoirs, which can host varying fractions of melt and aqueous fluids
3) Deep reservoirs, e.g., as formed by underplating at the interface of the crust and upper mantle funneling new melt to midcrustal levels

Distribution of benchmarks of the monitoring network is a compromise among survey target, costs, accessibility, manageability, and safety. For example, a high-precision local network might capture the shallow feeder system but is unlikely to provide information about deep magma plumbing (Jousset and Okada, 1999).

Microgravity surveys

Gravity time series are obtained by time-lapse surveys whereby relative microgravity readings are obtained at individual benchmarks. These measurements then are related to a reference outside the area of interest. With the recent advent of portable absolute gravimeters, time-lapse observations also are possible by using absolute readings (Ferguson et al., 2008) or, where challenging environmental conditions disallow use of absolute gravimeters at all sites of the array, through a combination of absolute and relative gravity measurements (hybrid microgravimetry). Hybrid microgravimetry might be especially important in areas where there is no guarantee of temporally constant gravity at the reference site (Furuya et al., 2003b).

Repeated occupation of the network leads to gravity time series that are evaluated with respect to data obtained at the reference. Consequently, one obtains a series of baseline readings between the reference and each survey benchmark. Obviously, baseline corrections are redundant if an absolute gravimeter is part of the survey network. Complexities arise, particularly on small volcanic islands, where it might be difficult to install a reference outside the zone of interest (Furuya et al., 2003b). Locating a reference too close to the target volcano causes serious ambiguities as to subsurface processes because deep-seated mass/density changes affect gravity measurements at both the reference and the network baselines.

Measurement errors are affected not only by the type of field gravimeter and operator but also by site effects such as benchmark stability and noise and by environmental effects from local pressure and temperature changes. To minimize environmental effects, gravity meters are sealed; thus, barometric-pressure changes should not affect the buoyancy of the mass. In addition, the measurement chamber is kept at constant temperature (thermostated). If a meter varies from its thermostated temperature, there will be intolerable instrumental drift. Each instrument is thermostated at a different temperature. In cold climates, using a meter that is thermostated at lower temperatures will conserve battery power. In hot climates, a meter that is thermostated at a higher temperature is less likely to go over temperature (LaCoste & Romberg, 2004).

The standard pressure correction between pressure and gravity (barometric-pressure admittance) usually is small, close to -0.3 μGal/mbar. Because this effect varies with both time and frequency, the contribution is spread over the full spectral domain and might inhibit the observation of small signals (on the order of nGal or a few μGal) of geophysical origin. This is especially important for high-precision measurements that can be obtained by superconducting gravimeters (Boy et al., 1998).

Using a Scintrex CG3-M gravimeter, Budetta and Carbone (1997) found a precision of between 3.5 and 4.4 μGal (1 μGal = 10^{-8} m/s^2) under various field conditions. Over a series of baseline readings, error propagation can add up to uncertainties of approximately 10 μGal (Battaglia et al., 2003b). For example, using a global navigation satellite system (GNSS)/GPS for benchmark elevation control and accounting for uncertainties in positioning of 2 to 3 cm in the vertical readily yields a precision of approximately 15 μGal for individual gravity baselines (Gottsmann and Battaglia, 2008).

Significant uncertainties in the reduction of gravity data usually are associated with tidal correction. Solid-earth tides (SET) are predictable to within reading precision of modern gravimeters, but ocean-loading (OL) contributions to gravimetric data can affect the precision of 4D gravimetric data dramatically (Berrino and Riccardi, 2001) and generally are large near coastlines with complicated bathymetry (Van Dam et al., 2007). Despite the availability of numerous OL models, local effects on volcanic islands cannot be predicted accurately enough. Loading depends on the immediate submarine topography around an island and the shape of the coastline; generic global models fail to account for such local effects (Arnoso et al., 2006). As a consequence, each benchmark of a network covering a small island might suffer from individual OL effects. Ideally, one would construct a tidal correction model for each benchmark, but this is not achievable in volcano-monitoring programs now or for the foreseeable future. A local model (applicable to the entire net-

work) to reduce residual OL effects could be constructed from tidal gravity data obtained from a permanently recording gravimeter operated as a tidal meter.

In the absence of precise SET and OL model data, reduction may be performed using data from a continuous gravity station operated in addition to a campaign meter over the period of the survey (Gottsmann and Battaglia, 2008). Alternatively, the network could be occupied with multiple gravimeters and operators to try to deduce the correct gravimetric baseline values statistically. However, in many cases, neither is achievable because of lack of infrastructure, equipment, and/or personnel. If only one meter is available for a survey, a way to account for uncertainties from OL is to propagate tidal-correction errors directly (e.g., at Montserrat, this uncertainty is up to 10 μGal; Figure 1a) or to avoid benchmark reoccupation on periods that match the half-width of OL periods.

Ocean-loading effects are particularly dominant over periods of approximately 12 hours (peak to peak, semidiurnal effects). Data contamination cannot be avoided entirely, but its effects can be reduced significantly by doing a baseline loop as quickly as possible, including initial measurement at the reference and at the benchmark and reoccupation of the reference (within approximately 3 hours). If gravimetric signals are expected to be significantly more than tidal uncertainties, errors can be propagated. However, most gravity changes at active volcanoes reported in the literature are on the order of tens of μGal; thus it appears reasonable to minimize errors from individual contributions, including tidal effects.

Time-lapse microgravimetry

After correcting for tidal effects, the observed gravity change g_{obs} is the difference in gravity along a baseline (between benchmark and reference). Under ideal conditions, resolvable gravity changes might be detectable up to 10 km from the region of maximum ground deformation if the mass change at depth is at least 10^{12} kg (Williams-Jones and Rymer, 2002). To extract the gravity signal produced by a subsurface mass and/or density change, gravity residuals must be quantified (Eggers, 1987). The residual gravity change at each benchmark Δg_r is given by

$$\Delta g_r = \Delta g_{obs} - \gamma \cdot u_z - \Delta g_{def} - \Delta g_{wt}.$$
(1)

Here, Δ denotes a gravity difference over time at the site [e.g., $\Delta g_{obs} = g_{obs}(t_2) - g_{obs}(t_1)$]; γ is the free-air gravity gradient (the value of the theoretical gradient γ_T is -308.6 μGal m^{-1}); u_z is the vertical displacement (positive for relative uplift and negative for relative subsidence); Δg_{def} is the Bouguer effect of deformation (the contribution of the volume change arising from compressibility of the medium surrounding the source, which also implies displacements of density boundaries in heterogeneous media); and Δg_{wt} is the effect of groundwater-table variation (Figure 1b). The source's geometry significantly affects the Bouguer reduction for the effect of deformation Δg_{def}. A spherical symmetry (Rundle, 1978; Walsh and Rice, 1979) results in the correction being exactly

zero. Deformation effects from a prolate spheroid are negligible, whereas deformation effects can be up to 80% for a horizontal penny-shaped crack source (Battaglia et al., 2006).

Critical to interpretation of residual gravity variations is the correction for Δg_{wt} (Battaglia et al., 2003b) or gravity changes induced by an active hydrothermal system (Gottsmann et al., 2007). The former correction can be approximated by

$$\Delta g_{wt} = 2\pi G \rho_w \phi \delta z,$$
(2)

where $2\pi G \rho_w = 42$ μGal m^{-1}, G is the universal gravitational constant 6.673×10^{-11} N m^2 kg^{-2}, ϕ is effective porosity, ρ_w is the density of water, and δz is the vertical water-table change for an unconfined aquifer. Gravity signals from shallow hydrothermal systems require installation of a tidal meter to correct for short-term fluctuations in aquifers (Gottsmann et al., 2007).

Failure to account for shallow sources might result in an inability to differentiate between gravity signals from changes in the magmatic plumbing system and those from background noise (e.g., water table) (Jachens and Roberts, 1985). As a result, the entire gravitational signal is attributed to deeper (usually magmatic) processes, and conclusions drawn then might be unrealistic.

Data aliasing

Aliasing effects in gravimetric data are important error sources. Although spatial aliasing plays a more important role during static
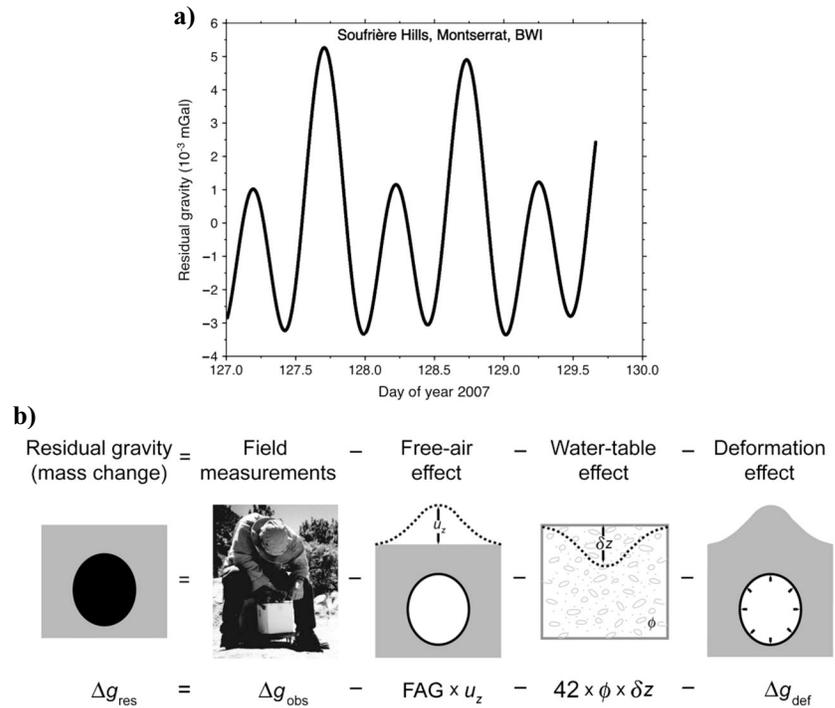

Figure 1. (a) Effect of OL. The figure shows the residual-gravity trace recorded 4 km from Soufrière Hills Volcano, Montserrat, British West Indies, during a period of dome-growth stagnation in June 2007 that was related predominantly to semidiurnal OL effects at this small volcanic island. Such time series are indispensable for precise reduction of gravimetric time-lapse observations and other geodetic observations to assess subsurface changes during eruption. (b) Different effects that compose the gravity signal measured in the field. All constants are in μGal m^{-1}; u_z is vertical displacement, FAG is the free-air gradient, ϕ is porosity, and δz is water-table change. (Modified from Battaglia et al., 2003b).

(time-independent) surveys, gravimetric-time-series data from time-lapse microgravity surveys might suffer distortion when data between individual surveys are compared. With benchmark occupation typically ranging from a few months to a few years, gravity variations detected between individual surveys might be caused by fundamental mass/density variations over much shorter time periods. The frequency that corresponds to the sampling interval of periodic surveys might be far lower than that of dynamic changes at depth, leading to a misrepresentation of timescales of subsurface dynamics.

Consequently, the real period of the signal (and thus any hypothesis about its source) might not be resolved unambiguously in the time domain because of the Nyquist limit. However, assuming that sources that evolve more quickly are shallower, this ambiguity could be tentatively solved in the space domain if the available network of stations is dense enough to allow distinction between effects linked to sources at different depths. Alternatively and ideally, coupling time-lapse observation on an extended network with continuous measurements at one or more selected sites can provide essential insights into mass/density variations at depth over both time and space (Carbone et al., 2003b). (See the "Continuous gravity" section below.) Interpretation of time-lapse data from a few annual or multiannual surveys therefore must be based on a cautious evaluation of timescales, especially in volcanic areas where active hydrothermal systems and magma reservoirs might operate over different periods.

A fundamental assumption for quantifying residual gravity changes is that ground deformation and gravity changes occur instantaneously because of a subsurface disturbance, resulting in a linear gravity-height signature. However, this linearly elastic assumption sometimes does not hold true (e.g., with time-dependent properties of volcanic reservoirs, such as viscoelastic relaxation of stress buildup (Yu et al., 1996). The resultant source parameters inferred from inverting geodetic and gravimetric data thus depend heavily on the assumption about mechanical properties of the host rock. See the "Analytical modeling" and "Numerical modeling" sections for more detail.

CONTINUOUS GRAVITY

As stated in the "Field setup and survey design" section, the usual repetition rate of discrete gravity observations limits the information about the development rate of the underground mass redistributions, often implying an ambiguity about the nature of the driving processes. Furthermore, weather during winter prohibits gravity changes at summits of higher volcanoes from being identified by discrete measurements (Carbone et al., 2003b). Using continuous gravity measurements helps to overcome these drawbacks and reduces the exposure of personnel in active areas during paroxysmal (potentially dangerous) activity. (See also Williams-Jones et al., 2008.)

For attaining appropriate precision with continuously running gravimeters, an ideal site is easily accessible (for checking the instrumentation frequently) and has small microseismic disturbance and very small temperature and pressure variations (Torge, 1989). Nevertheless, on an active volcano, the instruments are placed where there is the greatest chance of detecting meaningful gravity changes, which might only be close to an active crater (Branca et al., 2003; Carbone et al., 2008). Conditions at such a site (high altitude, inaccessibility for several months at a time, lack of electric power supply, high peak-to-peak diurnal and seasonal temperature changes, high seismicity) are far from the required standard. These constraints dictate that only spring gravimeters (Rymer, 1989; Budetta and Car-

bone, 1997) be used for the set-up because they are small (easier to transport and install) and need limited power (can operate using energy from solar panels and batteries).

Recent technological improvements allow station designs that overcome at least some of the difficulties linked to site inadequacy (Carbone et al., 2003b). However, the effect of meteorological parameters (De Meyer et al., 1995; El Wahaby et al., 2000) at a remote station is unavoidable because the reduced power supply prevents use of an active system to stabilize temperature, pressure, and humidity. The only possibility is to continuously measure the parameters that can perturb the gravimeter and to try to remove their effect from the gravity signal afterward.

The instrumental drift can be modeled as a first-degree curve, whereas the earth-tide and tilt effects are removed from the gravity signal using appropriate theoretical models (Carbone et al., 2003b).

The instrumental effect from ambient temperature

Ambient-temperature changes can affect the behavior of spring gravimeters dramatically. El Wahabi et al. (1997) found that over a year, temperature changes can cause an instrumental effect (noise) of up to 10^3 µGal. Using three spring gravimeters that were installed side-by-side at a site where gravity changes of geodynamical origin were not expected, Andò and Carbone (2004) demonstrate that the admittance and the phase of the instrumental effect from ambient temperature are instrument-specific. Furthermore, using records from the same instrumental setup, operating in different monitoring sites, Andò and Carbone (2006) found that the installation setup (in a broad sense) has an important influence on the transfer function between temperature and temperature-driven changes to instruments. Affecting parameters could be the construction material of the host site, the type of insulation used, and/or the microclimatic conditions of the installation site.

To investigate the relationship between the gravimeter output and ambient temperature, Andò and Carbone (2001, 2006) performed spectral-correlation analyses using a Matlab signal-processing toolbox, which is based on Welch's averaged-periodogram method (Welch, 1967). They calculate the coherence function, which indicates how well the meter output corresponds to the temperature at each frequency, and which is given by

$$C_{xy} = \frac{|P_{xy}|^2}{P_{xx}P_{yy}}, \tag{3}$$

where P_{xy} represents cross-spectral density and P_{xx} and P_{yy} represent power-spectral density. Using this approach, Andò and Carbone (2001, 2006) found that a significant correlation (coherence value between 0.6 and 0.8) appears just over the lowest frequencies (periods longer than approximately 10 days), with admittances of up to 0.2 mGal/°C (Carbone et al., 2003b).

Thus, apparent gravity changes caused by ambient-temperature fluctuations have varying character and magnitude, depending on the temporal development and magnitude of the meteorological change itself and on the characteristics of each gravimeter and installation site. Accordingly, the correction formulas are frequency-dependent and instrument/setup-specific and thus must be established case by case using nonlinear techniques. Andò and Carbone (2004) demonstrate the potential for a neurofuzzy algorithm to reduce continuous gravity sequences for the effect of ambient temperature. However, any fuzzy-model structure must be optimized (so-called "training process") using time series that are much longer than the

period of the influencing temperature fluctuations. In most cases, the unavailability of time sequences longer than one year implies that only the effect of temperature fluctuation with a period of up to a few months can be compensated for. Because in such cases it is not possible to resolve the ambiguity affecting the longest-period component of the gravity signals, it must be removed by using low-order polynomial fits (Bonvalot et al., 1998). This implies the risk of removing the "useful" signal along with the undesired one. A good way to minimize the amount of useful signal that is removed is to "calibrate" the order of the polynomial fit by comparing the results of the filtering process with gravity data acquired discrete gravity measurement at a site very close to the continuously running station (Andò and Carbone, 2001; Carbone et al., 2003b).

The instrumental effect from atmospheric pressure

Besides the real gravity effect caused by the gravitational attraction of the air column and the distortion of the earth's surface from barometric changes, which is easily removable using the standard admittance coefficient (-0.365 µGal/mbar) (Merriam, 1992), atmospheric-pressure changes also have been shown to induce instrumental effects on continuously recording Scintrex CG-3M gravimeters. Bonvelot et al. (1998) demonstrate that the internal temperature (inside the thermostated, air-tight chamber hosting the gravity sensor) of older-aged CG-3M meters — which have a less-robust acquisition system than later models — can be affected by atmospheric-pressure changes, probably because some electronic components of the acquisition system are sensitive to pressure variation. Apparent changes in internal temperature turn into apparent gravity changes because through their own software, these instruments reduce the gravity signal in real time on the basis of the recorded internal temperature. This shortcoming can be overcome by performing a correlation analysis between instrument internal temperature and atmospheric pressure and, if a significant correlation is found, reducing the thermal signal for the pressure effect and recomputing the correction to be applied to the gravity signal.

Bonvelot et al. (1998) also prove that atmospheric pressure can induce an effect on the tilt meters of Scintrex CG-3M instruments because of distortion of the external enclosure of the gravimeter. These apparent tilt changes induced apparent gravity changes that were lower than 1 µGal (Bonvelot et al., 1998) and thus are negligible when volcano-related gravity changes are the target.

To our knowledge, gravimeters other than the Scintrex CG-3M (older models) are not subject to instrumental effects from atmospheric pressure.

The potential of continuous gravity studies

The difficulty of compensating the gravity signal for the effect of ambient temperature does not unduly compromise the potential of continuous gravity measurement using spring gravimeters.

At Merapi volcano (Java, Indonesia), Jousset et al. (2000) installed a gravity station 4 km from the summit, inside a temperature-controlled room at the Babadan observatory. When using a thermo-insulating box to improve the gravimeter thermal isolation, temperature fluctuations can be restricted to within $0.3°C$ to $1.0°C$. During the two-year acquisition (1993–1995), they show that volcano-related gravity changes exceeded the instrumental noise because of temperature changes. Both for long terms (few months) and short terms (few days), they found clear correlations between residual gravity, seismicity, and volcanic activity (Jousset et al., 2000). In particular,

they show that residual-gravity decreases corresponded to intensive seismic activity (low-frequency events) and the occurrence of pyroclastic flows. The authors concluded that internal-pressure variation caused by crystallization and gas release to the surface could explain the gravity variations observed at Babadan, and they suggest that pyroclastic flows and dome collapse could be forecast by using continuous gravity monitoring.

When ambient-temperature changes cannot be restricted to an acceptable range (e.g., because of lack of adequate facilities to host the sensors), continuous gravity measurements still hold considerable potential. In fact, some authors demonstrate that the dynamics of volcanic and hydrothermal systems can cause measurable gravity changes over periods of between minutes and days (Branca et al., 2003; Carbone et al., 2006, 2008; Gottsmann et al., 2007).

Study of gravity changes that develop over short periods has two main advantages: (1) these changes should not be affected by temperature fluctuations, and (2) over short periods, the instrumental drift of spring gravimeters exhibits an overall linear behavior (Torge, 1989) and thus can be easily removed from the gravity time series. Short-period gravity changes are valuable both for studying the dynamics of the systems that cause them and for forecasting paroxysmal events.

At Mt. Etna (Italy), a gravity sequence that encompassed the breakout of the 2002 NE-Rift eruption was acquired at a summit station only 1 km away from the upper part of the newly forming fracture field (Branca et al., 2003). A marked gravity decrease of approximately 400 µGal in less than one hour was observed. This anomaly reversed at an even higher rate just before lava was first emitted from the eruptive fissures downslope (William-Jones et al., 2008). Branca et al. (2003) conclude that at least a part of the gravity decrease reflects a local mass decrease caused by the opening of the shallow fracture system very close to the gravity station. This conclusion rules out magma overpressure as a cause of the upper-fracture opening and indicates instead that magma from the central conduit entered the new fracture system passively, using it as a path to the eruptive vents downslope. Thus, the gravity sequence is the only evidence that can inform us about the intrusive mechanism that triggered Mt. Etna's 2002 NE-Rift eruption.

In the framework of multiparameter geophysical experiments at Nisyros caldera (Greece), residual gravity changes of up to 35 µGal from peak to peak were observed over periods of 40 to 60 minutes (Gottsmann et al., 2005, 2007). When cross analyzed with other available data (ground-deformation and seismic and electromagnetic data), these gravity fluctuations were found likely to be caused by degassing-process instabilities inducing thermohydromechanical disturbances of the hydrothermal system. The potential for continuous gravity studies to detect these instabilities means that through longer experiments, the geophysical signature of such processes, which can tip the system from background to paroxysmal activity, can be assessed.

During the 2002–2003 eruptions and the December 2005–January 2006 noneruptive period, gravity changes that negatively correlated with the tremor amplitude were observed in the summit zone of Mt. Etna (Carbone et al., 2006, 2008). These changes had amplitudes of 10 to 30 µGal and occurred over periods of a few hours.

In particular, during temporary switches of the 2002–2003 eruptive activity from vigorous lava fountains to mild Strombolian explosions, marked gravity decreases were observed at the only available summit station simultaneously with tremor-amplitude increases (Carbone et al., 2006) (Figure 2). These changes in activity were

assumed to reflect collapses of the magma/gas mixture within the upper level of the system feeding the active vent. The collapsed column diminished gas flow to the shallowest levels of the discharge system to the atmosphere, creating conditions under which a foam layer forms (Jaupart and Vergniolle, 1988). By substituting denser material (magma), a foam layer can induce a local mass (gravity) de-
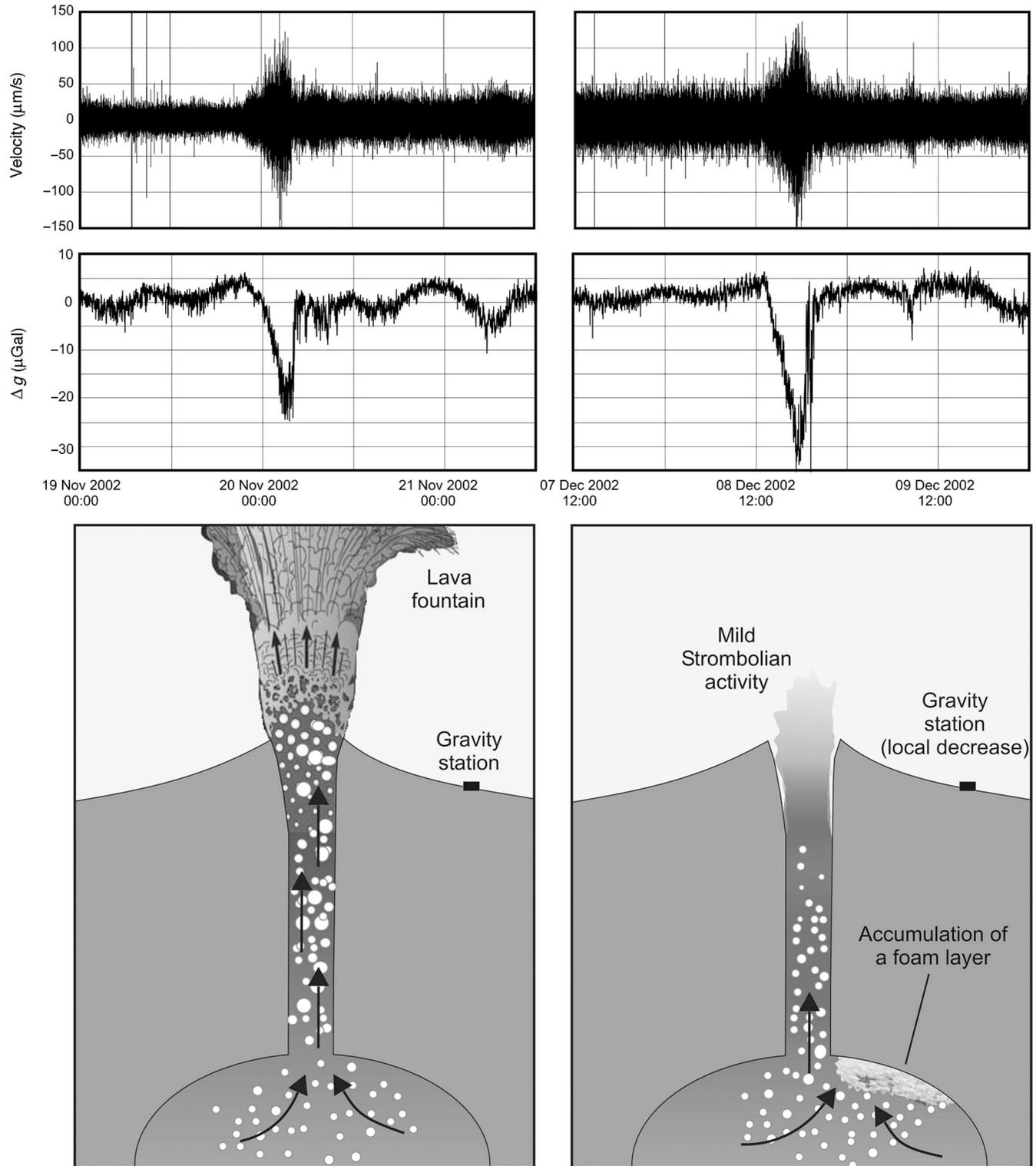

Figure 2. During the 2002–2003 Mount Etna eruption, gravity decreases lasting a few hours were observed simultaneously with increases in amplitude of the volcanic tremor. The joint tremor/gravity anomalies occurred during temporary switches from vigorous lava fountains to mild Strombolian activity. Carbone et al. (2006) interpret these anomalies as being caused by accumulations of foam layers during periods when gas flux along the upper part of the discharge system was inhibited. (See text for details.)

crease. It also can radiate seismic energy by coupled oscillations of the bubbles inside it. Growth of a foam layer thus could explain the observed joint gravity/tremor anomalies (Figure 2).

During the December 2005–January 2006 noneruptive period, tremor amplitude at Mt. Etna increased and negatively correlated with the gravity signal from one of the two summit stations that worked during that period, over 2- to 3-hour fluctuations (Carbone et al., 2008). No correlation was found with the signal from the other gravity station. In this case, by relying on the relative position of the two stations, it was possible to define the volume that contained the gravity source. During the period of marked anticorrelation, the tremor source (located by inverting the spatial distribution of seismic amplitudes) intersected this volume, lending support to the hypothesis that the anticorrelation marked the activation of a joint-source process. Relying on independent information, Carbone et al. (2008) suggest that this process was related to the arrival of fresh magma and the consequent gas separation, implying that the anticorrelated tremor/gravity anomalies were indicative of a system that was becoming progressively enriched in volatiles.

ANALYTICAL MODELING

Analytical models offer a closed-form description of the source of volcano unrest. This means that in principle, we readily may infer the relative importance of any of the source parameters. In active volcanic sites such as Long Valley caldera (California, U.S.A.) and Campi Flegrei (Italy), careful use of analytical models and high-quality data sets has produced good results. However, simplifications (e.g., the assumption that the crust is a homogenous, isotropic, elastic medium) that make analytical models tractable can lead to misleading volcanological interpretations, particularly in the case of structural discontinuities (Fernández and Rundle, 1994; Gudmundsson, 2006; Folch and Gottsmann, 2006). Constructing more-realistic (complex) models using numerical techniques requires introducing more model parameters. (See the "Numerical modeling" section.) The limited geodetic and gravity measurements available for most volcanoes might not provide the resolution needed to discriminate clearly between simple analytical models and more-complex numerical models for sources of volcano unrest. (See also De Natale and Pingue, 1996; Dvorak and Dzurisin, 1997; Dzurisin, 2003; Gudmundsson, 2006; and Lisowsky, 2006.)

Further complication arises if mass movement at depth does not cause ground deformation, such as with saturation of a permeable medium. There are cases of significant residual gravity changes without significant ground deformation and vice versa (Rymer et al., 1993; Carbone et al., 2003a), as well as of nonlinear relationships between gravity and deformation over a survey area (Gottsmann et al., 2006a, 2006b). These relationships sometimes are difficult to interpret (Battaglia and Segall, 2004), but several studies (Fernández and Rundle, 1994; Tiampo et al., 2004) suggest that gravitational coupling effects might be fundamental to explaining gravity changes at active volcanoes.

We present some of the analytical models that can be used to study unrest at central volcanoes and calderas that is caused by pressurization of magma or hydrothermal reservoirs at depth. The most common source geometries used to study this kind of deformation approximate the pressurized reservoir as a spherical, cigarlike, sill-like, or dike-like body.

The spherical magma chamber

The deformation caused by an expanding or contracting magma chamber has been modeled often using a dilatation source in an elastic half-space. Mogi's point source (McTigue, 1987) most commonly is used. The model simulates a small spherical expansion source embedded in a homogeneous, isotropic, Poisson-solid half-space (Figure 3a). The appeal of Mogi's model is its combination of computational simplicity and remarkable ability to fit real data quite well in many cases. However, the accuracy of an interpretation based on Mogi's model is subject to the validity of the assumptions (e.g., the source depth is significantly larger than its radius, the land surface is flat, Poisson's ratio $\nu = 0.25$, the crust is linearly elastic, and the role of pore fluids is negligible), an often-overlooked consideration (Masterlark, 2007). For example, Mogi's point-source model can explain stresses and displacements that are far from the chamber, but at the source, the stresses diverge to infinity. McTigue's (1987) formulation provides an analytical solution that includes higher-order terms taking into account the finite shape of a spherical body. Thus, the local stresses at and away from the chamber boundary can be calculated. McTigue's (1987) results for vertical deformation u_z and radial deformation u_r from a pressurized ΔP spherical magma chamber of radius b and depth d (Figure 3a) can be written in the form
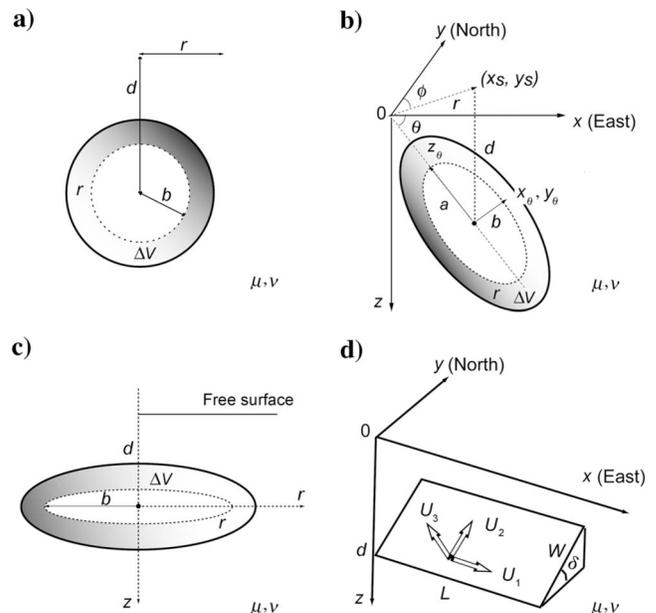

Figure 3. Geometry and parameters for source models. (a) A spherical source is described by four parameters: two for location (x_0, y_0), depth d, and volume change ΔV. (b) Prolate spheroids need seven parameters: two for location (x_0, y_0), depth d, volume change ΔV, aspect ratio A, dip angle φ, and strike angle θ. (c) A horizontal sill-like source is determined by five parameters: two for location (x_0, y_0), depth d, volume change ΔV, and radius b. (d) A dike is represented by six parameters: two for location (x_0, y_0), depth d, rectangular fault length L and width W, and dip angle φ. We can represent the strike-slip along the fault by the dislocation vector U_1, the dip-slip by U_2 and the tensile opening component by U_3 (after Okubo, 1992).

$$u_z = (1 - \nu)\frac{\Delta P b^3}{\mu}\frac{d}{(r^2 + d^2)^{3/2}}$$
$$\times \left\{ 1 - \left(\frac{b}{d}\right)^3 \left[\frac{1 + \nu}{2(7 - 5\nu)} - \frac{15(2 - \nu)}{4(7 - 5\nu)}\frac{d^2}{r^2 + d^2} \right] \right\} \tag{4}$$

and

$$u_r = u_z \frac{r}{d}, \tag{5}$$

where ν is Poisson's ratio, μ is the shear modulus, and r is the horizontal distance between the vertical projection of the source center and the observation point. The change in volume of the body ΔV is $\pi b^3 \Delta P/\mu$. McTigue's (1987) equations 4 and 5 reduce to Mogi's point-source formulation when $b/d \ll 1$. A direct consequence of the assumption of point of dilatation is that the magma chamber radius b and pressure change ΔP are inseparable in both the Mogi and the McTigue model because $\Delta P b^3$ is the strength of the point singularity (McTigue, 1987).

The gravitational attraction of a spherical magma chamber of finite size and mass $m = \rho \Delta V$, where ρ is magma density, is identical to that of a point magma chamber with the same mass m:

$$\Delta g_z = G\rho \Delta V \frac{d}{(r^2 + d^2)^{3/2}}, \tag{6}$$

where G is the universal gravitational constant. If the point-source approximation holds and the water table and deformation effects are neglected, then equations 4 and 6 can be combined to get a linear relationship for the density of the intrusion (Eggers, 1987):

$$\rho = \frac{1 - \nu}{G\pi}\left(\frac{\Delta g}{u_z} - \gamma\right), \tag{7}$$

where $\gamma = 308.6 \ \mu$Gal/m is the free-air gradient.

Pipelike sources

A simple model of a volcanic system includes two principal elements: a magma reservoir and a conduit through which the magma can reach the surface. When the volcano is quiescent, the conduit closes, allowing pressure buildup in the reservoir. The surface-deformation pattern caused by a cigar-shaped magma chamber is quite different from that from a spherical reservoir. Yang et al. (1988) formulated a model for a pressurized cigar-shaped magma body (Figure 3b). They found an approximate but very accurate solution for a dipping prolate ellipsoid in an elastic half-space using a half-space double force and center-of-dilatation solutions. Newman et al. (2006) reported minor corrections to the Yang et al. (1988) analytical model. Whereas the expressions in the near field are quite complex, the equations for the surface deformation for a vertical prolate ellipsoid become relatively simple in the far field (when the radial distance r is much larger than semiminor axis of the ellipsoid):

$$u_z = \frac{ab^2}{3\mu}d\left[\frac{2(1 - 2\nu)P^* - 2\nu P^\updownarrow}{R^3} + 3\frac{d^2 P^\updownarrow}{R^5} \right] \tag{8}$$

and

$$u_r = \frac{ab^2}{3\mu}r\left[\frac{2(1 - 2\nu)P^* - 2\nu P^\updownarrow}{R^3} + 3\frac{d^2 P^\updownarrow}{R^5} \right], \tag{9}$$

where a and b are the semimajor and semiminor axes of the ellipsoid, respectively; P^* and $P^\updownarrow$ are proportional to the pressure change ΔP (Yang et al., 1988, p. 4250); and $R^2 = r^2 + d^2$. The expression for the volume change of a pressurized spheroid is $\Delta V = \pi ab^2 \Delta P/\mu$ (Tiampo et al., 2000). The general solution for a prolate spheroid depends on seven parameters (Figure 3b): ΔP; the geometric aspect ratio $A = b/a$ between the semimajor axis a and the semiminor axis b; three parameters for the source location (x_0, y_0, d); the dip angle θ; and the azimuth angle ϕ, measured clockwise from the positive north direction.

The observed residual-gravity component for a prolate spheroid of density ρ is

$$\Delta g_z = G\rho \Delta V(3z_\theta f_1 \sin \theta - 1.5y_\theta f_2 \cos \theta) \tag{10}$$

(Clark et al., 1986), where the subscript θ indicates the coordinates with respect to the principal axes of the spheroid (Figure 3b). Note that for a vertical prolate spheroid ($\theta = 90°$), equation 10 reduces to

$$\Delta g_z = 3G\rho \Delta V d f_1. \tag{11}$$

Expressions for functions f_1 and f_2 are in Appendix A.

Sills

Sill-like magma intrusions or chambers can be represented by finite, pressurized, horizontal, circular cracks (Fialko et al., 2001) (Figure 3c). The exact expressions of Fialko et al. (2001) are appropriate for a sill-like source whose radius is up to five times greater than its depth. The expression for surface displacements has the form

$$u_j = \int_0^1 [K_\phi(r,t)\phi(t) + K_\psi(r,t)\psi(t)]dt \quad j = r,z, \tag{12}$$

where K_ϕ, K_ψ, ϕ and ψ are given in equation 27 and Appendix B of Fialko et al. (2001).

We can approximate the gravity changes caused by a sill-like mass by using a degenerate oblate spheroid (see Appendix A):

$$\Delta g_\theta^z = \frac{3G\Delta M d}{b^3}\left\{ \tan^{-1}\left(\frac{b}{\sqrt{\lambda}}\right) - \left(\frac{b}{\sqrt{\lambda}}\right) \right\}. \tag{13}$$

Dikes

A rectangular, tensile dislocation source that is based on an analytical expression developed by Okada (1985) for ground displacements and one by Okubo (1992) for gravity changes can be used to represent the crustal deformation and gravity changes associated with dike intrusion (Okubo et al., 1991; Furuya et al., 2003a).

The dike can be approximated by using a rectangular fault of length L and width W with dip angle δ at a depth d in a homogeneous, isotropic, elastic half-space (Figure 3d). We can represent the strike slip along the fault by the dislocation vector U_1, the dip slip by U_2, and the tensile opening component by U_3 (Figure 3d). Okada

(1985) gave formulas for the displacement for this fault model so that the vertical fault displacement Δh^{fault} can be easily estimated. Following the approach of Okubo et al. (1991), the gravity changes caused by faulting on a rectangular plane are

$$\begin{aligned} \Delta g^{\text{fault}}(x,y) = & \ \{\rho_c G[U_1 \times S_g(\xi,\eta) + U_2 \times D_g(\xi,\eta) \\ & + U_3 \times T_g(\xi,\eta)] + \Delta\rho G U_3 \times C_g(\xi,\eta)\}\| \\ & - \gamma\Delta h^{\text{fault}}(x,y), \end{aligned} \quad (14)$$

where ρ_c is the density of the crust, $\Delta\rho = \rho - \rho_c$ is the difference between the intrusion density and the crust density, and $\gamma\Delta h^{\text{fault}}$ is the free-air effect. Appendix A contains complete mathematical expressions for the functions in equation 14.

Gravity/height gradients

Gravity-height analysis also is a straightforward way to assess subsurface dynamics. Several applications and theoretical considerations of gravity-height signatures at active volcanoes were reported in Rymer and Williams-Jones (2000), Gottsmann and Rymer (2002), Gottsmann et al. (2003), and Gottsmann et al. (2006a).

Gravity and height changes are theoretically inversely correlated. A positive change in surface elevation (inflation) causes a net gravity decrease, expressed by the free-air gravity gradient γ. Ideally, γ will be measured directly because conclusions drawn from gravity changes caused by subsurface processes might be less meaningful if the value of the real free-air gradient deviates substantially from the theoretical gradient γ_T. Alternatively, if the local density anomaly is assumed to be caused by a point source, the local free-air gradient γ_a can be estimated from static gravity data (Rymer, 1994):

$$\gamma_a = \gamma_T - \frac{\Delta g_b(2z + 1)}{(z + 1)^2} \quad (15)$$

where Δg_b is the maximum amplitude of the Bouguer anomaly and z is the depth of the point source. At the Campi Flegrei caldera, for example, the calculated local gradient γ_a matched the measured gradient γ within error (Berrino et al., 1984; Berrino, 1994).

Gravity-height data that deviate from the theoretical gradient γ_T must be interpreted in terms of subsurface mass changes. No mass change is required for data that fall on this gradient, but a subsurface density change is necessary. If there is a mass change but no density change, the gravity-height data will follow the Bouguer-corrected gradient γ (γ_{BC}). The value of the corrected gradient γ_{BC} depends on the density ρ, the geometry of the source, and the value of the measured gradient γ (Rymer, 1994).

Fernández et al. (2005) described a method for computing and interpreting gravity and height changes and vertical gravity gradients produced by magmatic intrusions in a layered elastic-gravitational medium (Rundle, 1982; Fernández and Rundle, 1994). The theoretical elastic-gravitational model allows computation of geometric and orthometric vertical displacements and different types of gravity changes, as well as of the corresponding vertical gravity gradients. Their results showed that these gradients are useful for obtaining information about the dynamics of the injection processes, including detection of new magmatic intrusions and source-depth changes. By using the elastic-gravitational deformation model, they could explain nonlinear gravity-height relationships that appear in volcanic areas. Fernández et al. (2005) successfully used this method to infer the intrusion of new magma beneath Mayon volcano (Philippines). Their inference was confirmed when Mayon volcano erupted in July

2006. Gottsmann et al. (2006a) applied this methodology to observations at Campi Flegrei caldera to test source multiplicity.

Long Valley caldera

Careful use of analytical models and high-quality data sets can produce reasonable results. For example, through the combined use of geodetic and gravity data, Battaglia et al. (2003a, 2003b) were able to constrain the density of the intrusion beneath the Long Valley caldera resurgent dome. Their work provided guidelines for several problems that are common to volcano geodesy: (1) measuring the uplift by differencing GPS-based and leveled orthometric heights; (2) determining a unique geometry for the source (e.g., Dietrich and Decker, 1975); and (3) obtaining realistic estimates of the source parameters' uncertainties. For example, the standard approach of fitting the data to a point source will produce biased results if the true source does not possess spherical symmetry. Therefore, Battaglia et al. (2003a) used a combination of vertical and horizontal geodetic measurements (GPS, leveling, and line-length data) to find the best-fitting source geometry, in their case, a vertical prolate ellipsoid. When that source geometry had been uniquely determined, they performed a joint inversion of the uplift and gravity data to infer the volume and mass of the source, and completed a statistical analysis to assess the impact of data uncertainties on the density (Battaglia et al., 2003b). The source's estimated density range was 1180 kg/m^3 to 2330 kg/m^3. Because this density range is too high for hydrothermal fluids to be the sole source of uplift at Long Valley, the authors concluded that a silicic magma body or a combination of magma and hydrothermal fluids must have produced the observed deformation.

NUMERICAL MODELING

In volcanology, numerical models have been developed mostly to compute displacements produced by magmatic intrusions into elastic (Dietrich and Decker, 1975; Cayol and Cornet, 1998; Williams and Wadge, 2000; Bonaccorso et al., 2005; Lungarini et al., 2005) or viscoelastic media (Folch et al., 2000; Trasatti et al., 2003). Most of these studies account for the effect of topography and rheological heterogeneities on deformation. However, a few studies apply numerical methods to model deformation and gravity changes produced by magma intrusions, using 3D indirect boundary element method (IBEM) (Charco et al., 2007c) or finite-element method (FEM) (Currenti et al., 2007).

The effect of topography

Several studies on the topographic effect (McTigue and Stein, 1984; McTigue and Segall, 1988; Cayol and Cornet, 1998; Williams and Wadge, 1998; 2000; Folch et al., 2000; Charco et al., 2002; Trasatti et al., 2003; Lungarini et al., 2005) support the conclusions that topography has a significant effect on the deformation field and that in many cases the flat half-space approximation could lead to erroneous interpretation of observed ground deformation.

When computing volcanic loading effects, coupling between gravity and elasticity is negligible for displacements in the spatial scale associated with volcano monitoring, but the absolute effects of the existing gravity field become important when rigidity decreases (i.e., viscoelastic media) (Fernández et al., 1997; Battaglia and Segall, 2004; Charco et al., 2006). Coupling is a second-order effect that cannot be ignored in flat half-space models when a mass source term

(see, e.g., Rundle, 1980, 1982; Fernández and Rundle, 1994; Fernández et al., 2001a, 2001b; Fernández et al., 2006) represents the emplacement of magma at some depth. The mass and its interaction with the surrounding medium can vary the pattern of gravity change and produce measurable gravity anomalies. Thus, elastic-gravitational half-space models can provide a suitable approximation to problems of volcanic loading in areas where topographic relief is negligible. For prominent volcanoes, the rough topography has greater effect than does self-gravitation (Charco et al., 2007a, 2007c). In these cases, self-gravity can be ignored, whereas the topographic effect on displacements and gravity changes must be computed.

Starting from these theoretical results, Charco et al. (2007b) computed displacement and gravity changes produced by volcanic loading (internal loading produced by pressure and mass changes). To represent the displacement field that was perturbed by 3D topographic features, they used a single-layer boundary integral derived from Betti's reciprocal theorem and the solution to Kelvin's problem of a point load in an infinite body (Sánchez-Sesma and Luzón, 1995). Accounting for topographic effects, they computed the surface gravity change g_s as

$$g_s = \gamma(u_{zp} + u_{zm}) + \frac{GMc'}{R'^3}, \qquad (16)$$

where γ is the free-air gradient; u_{zp} is the vertical displacement caused by a massless (cavity) pressure source; u_{zm} is the vertical displacement produced by a constant-volume (pressureless) mass source (see Figure 1b); $R' = [(x - s_1)^2 + (y - s_2)^2(z - c')^2]^{1/2}$, with (x, y, z) being the coordinates of the calculation point and (s_1, s_2, c') being the coordinates of the source (point magma intrusion M); and $c' = c + z(x,y)$, where c is the source depth below mean sea level and $z(x,y)$ is a function of the computation-point horizontal location that represents the elevation above mean sea level. In this approach, topographic contributions to the gravity changes are implemented numerically through the change in vertical displacement and by considering the variation of the gravitational attraction of the mass.

Charco et al. (2007b) carried out several theoretical tests and applied the numerical model to Teide volcano (Tenerife, Canary Islands), taking into account the real topography (represented by a digital elevation model). They showed that the magnitude and the pattern of the gravity signals are significantly different from those of half-space solutions, as is the case for displacement. Figure 4 shows some of the results obtained by Charco et al. (2007b) for Teide volcano.

The effects of heterogeneities

Currenti et al. (2007) used FEM to model ground deformation and gravity changes produced by volcanic-pressure sources and to investigate the effects of topography and medium heterogeneities. By applying finite-element analysis, they were able to account for the real topography and elastic heterogeneities and thus to appraise their effects on the computed fields. Currenti et al. (2007) defined the gravity changes caused by pressure changes as

$$\Delta g = \Delta g_0 + \Delta g_1 + \Delta g_2 + \Delta g_3, \qquad (17)$$

where Δg_0 represents the free-air gravity change, Δg_1 arises from displacements of density boundaries in heterogeneous media, Δg_2 denotes the contribution of the inflation source, and Δg_3 is the contri-

bution to the gravity change from density variations in the surrounding medium. The authors stress that gravity changes cannot be interpreted in terms of additional mass input only, disregarding the deformations of the surrounding rocks (Bonafede and Mazzanti, 1998; Charco et al., 2007b).

Currenti et al. (2007) solved the model equations in two steps. First they solved the deformation field in terms of elastostatic-equilibrium equations, computing displacement and stress fields. Then they computed the solution for the coupled problem for the gravity field, in which the solutions of the deformation field are used to compute Δg_1, Δg_2, and Δg_3 contributions. They ran theoretical tests to find ground-deformation and gravity-field discrepancies between results from analytical expressions (Hagiwara, 1977), which disregard topography, elastic heterogeneities, and density subsurface structures, and results from numerical modeling, which takes these parameters into account.

Currenti et al. (2007) also review the gravity changes and ground deformation at Mt. Etna during the 1993–1997 period, assuming an ellipsoidal pressure source expanding in a heterogeneous medium with real topography. They show that heterogeneity and topography engender deviations from analytical results for a homogeneous plane medium. They also found that perturbations are more evident in the presence of severe heterogeneities and steeper topography, as is the case for the volcano's summit. Charco et al. (2007b) obtained a similar result for topographic effects and previous models for deformation (Williams and Wadge, 1998). Currenti et al. (2007) found that elastic heterogeneity affects only the magnitude of the anomalies, whereas topography greatly changes anomalies' magnitude and shape, especially in the Δg_1 contribution. They show that neglecting layering and topography leads to underestimation of elevation and gravity changes. One limitation of their work is that they only consider pressure changes as the source of unrest; they ignore the effect of the mass of the magmatic intrusion on the geodetic signature. Fernández and Rundle (1994) and Fernández et al. (1997) obtained similar results on medium heterogeneity for point sources and layered media.

Elisa Trasatti and Maurizio Bonafede (personal communication, 2008) used FEM to investigate gravity changes and uplift at Campi Flegrei. First they computed displacement and strain fields. Then they used the results to integrate the gravity variations numerically. They separate the observed gravity change into parts that correspond to the elevation change (free-air gravity change Δg_{FA}) and that were produced by mass redistribution (residual gravity change Δg_R):

$$\Delta g = \Delta g_{FA} + \Delta g_R. \qquad (18)$$

With similar considerations to Currenti et al. (2007), they expressed residual gravity change as

$$\Delta g_R = \Delta g_s + \Delta g_M = \Delta g_s + \Delta g_V + \Delta g_L, \qquad (19)$$

where Δg_s depends on the density change related to the introduction of new mass, Δg_M is the contribution from deformation of the medium that surrounds the source, Δg_V depends on the finite compressibility of rocks and vanishes if the medium is incompressible, and Δg_L is produced by density changes within the medium and accounts for the nonhomogeneities of the medium. The expression for Δg_L depends on whether the material density varies continuously or discontinuously in the reference configuration.

E. Trasatti and M. Bonafede (personal communication, 2008) began by considering a homogeneous, elastic, isotropic medium, and

later introduced density or rigidity variations and inelastic models. They also considered different source geometries (Mogi sources, spheroid, and sill). Their results confirm previous results regarding the control that the source geometry has on the deformation (Dieterich and Decker, 1975). Nonspherical sources yield positive and neg-

ative gravity changes (corresponding to sill and spheroid, respectively) without input of new mass. E. Trasatti and M. Bonafede (personal communication, 2008) pointed out the importance that source shape and the medium's characteristic has for gravity calculation and source-density estimation.
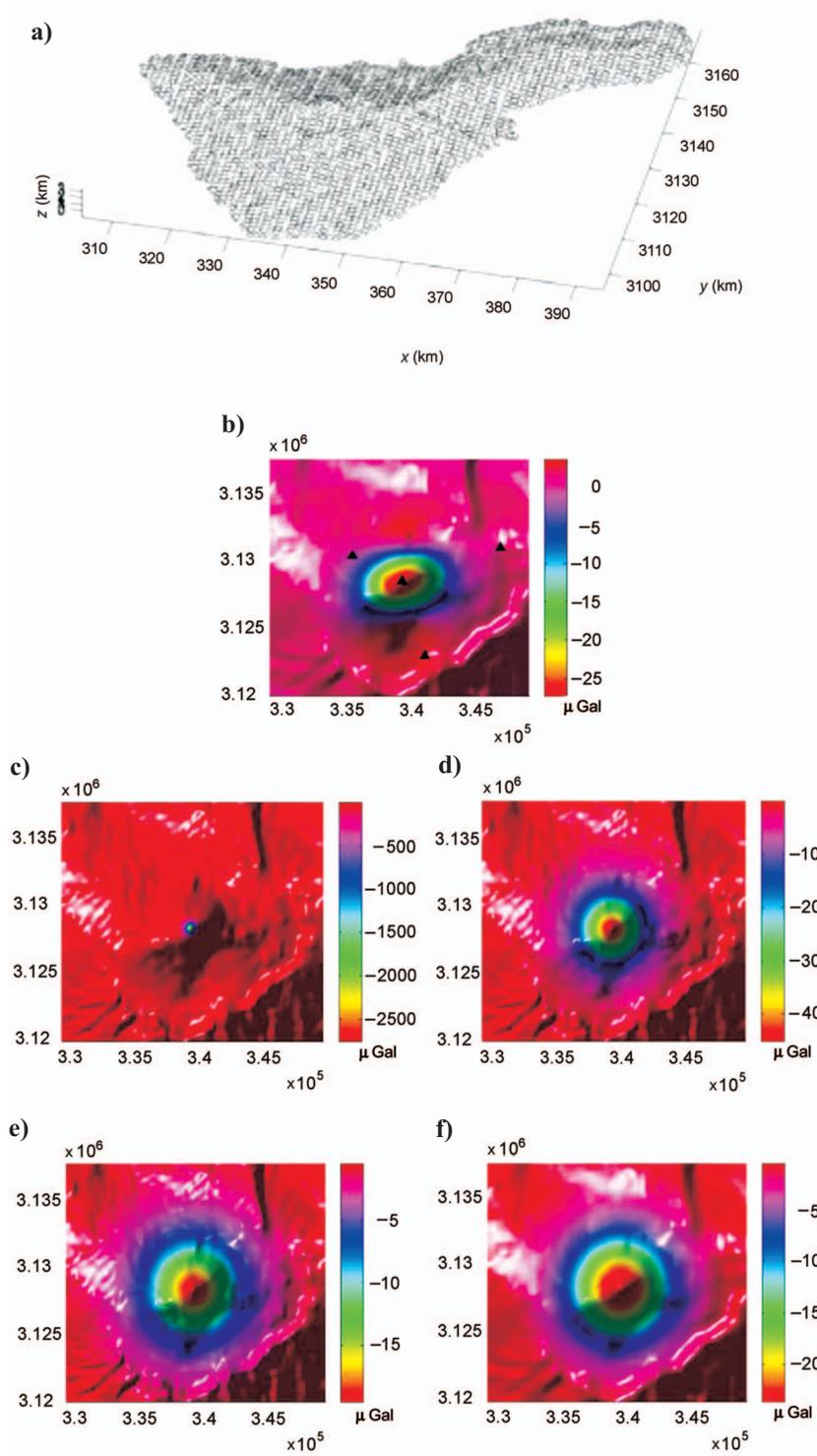
Figure 4. (a) Mesh of the Tenerife ground surface, formed by 2902 circular and flat elements that cover the whole island, and surface gravity change g_s caused by a center of dilatation of 50-MPa km^3 strength. Subplots (b) through (f) are gravity calculations, computed as follows: (b) using IBEM for the source located at 4 km below the Teide volcano summit, approximately 300 m below sea level; (c) using the analytical Mogi model, in which the top of the half-space is at sea level and the topography of Tenerife Island is neglected completely; (d) using the analytical Mogi model and assuming a reference elevation of 2700 m above sea level; (e) using the analytical Mogi model with the top of the half-space at 3718-m height, which is the Teide volcano height; and (f) approximating the island as an axisymmetrical cone with a height equal to that of the Teide volcano and with average slope of the flanks of 16.5°. In the last case, IBEM was used and the mesh was made up of 2561 circular elements. It can be seen that characteristics (pattern and magnitude) of the gravity variation field are very different when considering flat surface and topography. The main difference between real and approximate topography consideration is the pattern of the gravity variation. Horizontal coordinates for panels (b) through (f) are UTM coordinates in meters (modified from Charco et al., 2007a).

DISCUSSION

Microgravity observations furnish valuable information about volcanic processes that precede large eruptions and/or potentially dangerous paroxysms. Because it is linked intimately to the redistribution of underground masses, this information often is difficult to retrieve with other geophysical and geochemical techniques.

Microgravity observations at active volcanoes usually are conducted through repeated (discrete) measurements along an array of stations in the zone of interest and one (or a few) reference station(s) outside the active area. To be most suitable, a station network must be designed to satisfy the needs of monitoring programs. It also is important to rigorously apply the best strategies for reducing the effects in the gravity data that are related to instrumental drift, earth tide, ocean load, and water table.

Over the past few decades, analytical solutions have been derived and widely used to model the source mechanisms of volcano-related gravity changes. The potential for applying these formulations is greatly enhanced if gravity data are analyzed and interpreted jointly with simultaneous ground-deformation data. Phenomena-inducing unrest can be constrained regarding both the mass that is added to or withdrawn from the system and the stress that is induced in the medium that surrounds the source and that eventually is transmitted to the ground surface.

Because no one solution addresses how best to track mass variations beneath volcanoes, each case needs dedicated analysis. Observed gravity changes must be considered within the general context of available volcanological and geological observations. This facilitates choosing the most appropriate analytical formulation to describe the driving mechanism and thus helps in making assumptions about the shape of the source and the nature of the driving mechanism, based on other scientific evidence. The source parameters (size, position, amount and density of the redistributed mass, etc.) are then retrieved by fitting observed and calculated data through an appropriate inversion scheme. Many studies have proved that this approach can supply unique insights into the processes that lead to unrest (e.g., Battaglia et al., 2003b; Berrino, 1994; Bonafede and Mazzanti, 1998; Branca et al., 2003; Charco et al., 2007c; Currenti et al., 2007; Eggers, 1987; Fernández et al., 2001b; Furuya et al., 2003b; Gottsmann et al., 2005; Jachens and Roberts, 1985; Jousset and Okada, 1999; Okubo et al., 1991; and Rymer, 1994).

Major shortcomings of this approach are that the wrong model might be used to fit the observed data because different elastic models can produce similar effects, and that the simplifications (e.g., the assumption that the crust is a homogenous, isotropic, elastic medium) that make analytical models tractable can yield misleading volcanological interpretations.

More realistic (complex) models can be obtained by using numerical techniques, which allow the effects of topography and of medium heterogeneities to be accounted for at the cost of introducing more model parameters. It is worth stressing that the limited extent and density of the measurements usually available at most volcanoes does not provide adequate resolution to clearly discriminate between results from simple analytical models and more-complex numerical models. Thus, numerical models can be very useful for research but might be limited in their operative use during volcano-monitoring programs because of inherent complexities that prevent their straightforward and generic incorporation for inversion (interpretation) of observed deformation and gravity changes.

Campaign microgravity measurements also have intrinsic limitations related to data aliasing. Because temporal resolution of causative processes are two times the occupation interval (Nyquist frequency), which usually ranges from months to years, temporal characterization of causative source processes might be ambiguous. Since the 1990s, to overcome this restriction, continuous gravity measurements have been performed at active volcanoes. However, the cost of gravimeters (tens of thousands of dollars) has prevented deployment of extended arrays of continuous gravimeters.

Furthermore, the strong instrumental effect that is driven by atmospheric effects often prevents resolution of the ambiguity that affects the longest-period component of the gravity signal acquired by spring gravimeters. Thus, continuous gravity measurements are used either to integrate campaign data or to evidence quick changes (periods of minutes to days) linked to gas/fluid/magma dynamics over the shallowest part of the plumbing system. This implies that as of now, rather than quantifying the spatial evolution of gravity variations, the useful information that continuous gravity measurements can assess is the temporal evolution of fast-developing anomalies at one or a few sites close to the active structures. This information is increasingly acquired at some volcanoes; its rigorous interpretation requires new analytical and numerical models that account for the spatiotemporal evolution of volcanic systems.

CONCLUSIONS

Microgravity studies at active volcanoes can detect states of unrest with a degree of detail that other techniques cannot achieve. Retrievable information includes not only the source position and the amount of mass redistributed, but also the density of the material triggering the unrest and thus the nature of the causative source. As such, processes triggered by magma movements can be distinguished from mechanisms that are linked to the dynamics of gas or hydrothermal fluids. Enhancing the capabilities of this technique will require efforts on both the instrumental and the modeling aspects.

Once they become available, fully portable, low-energy-consumption and low-cost absolute gravimeters will make time-lapse microgravity surveys much more effective and easier to accomplish. On large volcanoes such as Mt. Etna, operators using absolute instruments will not be forced to reach "stable" reference stations that are far from the active areas, at the cost of propagating-measurement errors and greatly increasing measurement time. On small islands such as Montserrat and Stromboli, using an absolute gravimeter would overcome the potential reference instability when situated too close to the active zone. Even with absolute meters, it is ideal to have reference stations because there could be a larger background signal that could be aliased into a survey, such as postglacial rebound, that would be critical to quantify with a reference network.

Development of low-cost gravimeters (possibly not based on the spring-mass system) that are easily installable under harsh volcanic conditions and unaffected by ambient-temperature changes would promote wider use of continuous gravity measurements, which despite their promising potential still are not widely used as a volcano-monitoring tool.

Regarding data modeling, efforts are needed toward finding compromises between computational speed and precision in quantifying mass redistributions within volcanic systems to integrate numerical modeling into volcano-monitoring programs. Simulation schemes also are needed to evaluate the gravity effect (in terms of maximum

amplitude, duration, and time evolution) associated with fast-evolving volcanic processes such as convection, bubble growth, degassing, and aqueous-fluid migration.

APPENDIX A

MODELING GRAVITY RESIDUALS

Prolate spheroid

The observed residual-gravity component for a prolate spheroid of density ρ is (Clark et al., 1986)

$$\Delta g_\theta^z = 3G\Delta M z_\theta f_1, \quad \Delta g_\theta^y = 1.5G\Delta M y_\theta f_2,$$

$$\Delta g_\theta^x = 1.5G\Delta M x_\theta f_2,$$

$$f_1 = \frac{1}{(a^2 - b^2)^{1.5}}\left\{\left[\frac{a^2 - b^2}{a^2 + \lambda}\right]^{0.5}\right.$$
$$\left. - \log\left[\frac{(a^2 + b^2)^{0.5} + (a^2 + \lambda)^{0.5}}{(b^2 + \lambda)^{0.5}}\right]\right\}$$

$$f_2 = \frac{1}{(a^2 - b^2)^{1.5}}\left\{\log\left[\frac{(a^2 + b^2)^{0.5} + (a^2 + \lambda)^{0.5}}{(b^2 + \lambda)^{0.5}}\right]\right.$$
$$\left. - \frac{(a^2 + b^2)^{0.5}(a^2 + \lambda)^{0.5}}{(b^2 + \lambda)}\right\}, \quad \text{(A-1)}$$

where λ is the largest real root of cubic equation

$$\frac{z_\theta^2}{a^2 + s} + \frac{r_\theta^2}{b^2 + s} = 1, \quad r_\theta^2 = x_\theta^2 + y_\theta^2 \quad \text{(A-2)}$$

or

$$s^3 + p_2 s^2 + p_1 s + p_0 = 0, \quad \text{(A-3)}$$

where

$$p_2 = a^2 + 2b^2 - z_\theta^2 - r_\theta^2,$$
$$p_1 = 2a^2 b^2 + b^4 - 2b^2 z_\theta^2 - (a^2 + b^2)r_\theta^2,$$
$$p_0 = a^2 b^4 - b^4 z_\theta^2 - a^2 b^2 r_\theta^2. \quad \text{(A-4)}$$

The observed vertical component of the gravity acceleration (residual gravity) is

$$\Delta g_z = \Delta g_\theta^z \sin\theta - \Delta g_\theta^y \cos\theta$$
$$= G\rho\Delta V(3z_\theta f_1 \sin\theta - 1.5y_\theta f_2 \cos\theta). \quad \text{(A-5)}$$

Note that for a vertical prolate spheroid ($\theta = 90°$), equation A-5 reduces to

$$\Delta g_z = 3G\rho\Delta V d \cdot f_1, \quad \text{(A-6)}$$

whereas the observed gravity for a horizontal prolate spheroid ($\theta = 0°$) is

$$\Delta g_z = 1.5G\rho\Delta V d \cdot f_2. \quad \text{(A-7)}$$

Oblate spheroid

We can use a degenerate oblate spheroid to approximate gravity changes caused by a sill-like mass (Clark et al., 1986):

$$\Delta g_\theta^z = \frac{3G\Delta M z_d}{(b^2 - a^2)^{1.5}}\left[\tan^{-1}\left(\frac{b^2 - a^2}{a^2 + \lambda}\right)^{0.5} - \left(\frac{b^2 - a^2}{a^2 + \lambda}\right)^{0.5}\right]$$
$$\text{(A-8)}$$

In the limit of $a/b \to 0$, equation A-8 reduces to

$$\Delta g_\theta^z = \frac{3G\Delta M d}{b^3}\left(\tan^{-1}\frac{b}{\sqrt{\lambda}} - \frac{b}{\sqrt{\lambda}}\right). \quad \text{(A-9)}$$

Again, λ is the largest real root of the cubic equation A-3.

Dike

Following the approach of Okubo et al. (1991), the gravity changes caused by faulting on a rectangular plane are

$$\Delta g^{\text{fault}}(x,y) = \{\rho_c G[U_1 \times S_g(\xi,\eta) + U_2 \times D_g(\xi,\eta)$$
$$+ U_3 \times T_g(\xi,\eta)]$$
$$+ \Delta\rho G U_3 \times C_g(\xi,\eta)\}\| - \gamma\Delta h^{\text{fault}}(x,y),$$
$$\text{(A-10)}$$

where ρ_c is density of the crust, $\Delta\rho = \rho - \rho_c$ is the difference between the intrusion density and the density of the crust, and $\gamma\Delta h^{\text{fault}}$ is the free-air effect. The symbol $\|$ in equation A-10 stands for the Chimney's notation:

$$f(\xi,\eta)\| = f(x,p) - f(x,p - W) - f(x - L,p)$$
$$+ f(x - L,p - W), \quad \text{(A-11)}$$

where p is related to x_2 by

$$p = y\cos\delta + d\sin\delta. \quad \text{(A-12)}$$

(S_g, D_g, T_g, C_g) in equations 14 and A-10 are given by

$$S_g(\xi,\eta) = -\frac{q\sin\delta}{R} + \frac{q^2\cos\delta}{R(R + \eta)}, \quad \text{(A-13)}$$

$$D_g(\xi,\eta) = 2I_2(\xi,\eta)\sin\delta$$
$$- \frac{q(\eta\sin\delta - q\cos\delta)}{R(R + \xi)}, \quad \text{(A-14)}$$

$$T_g(\xi, \eta) = 2I_2(\xi, \eta)\cos \delta$$

$$+ \frac{q(\eta \cos \delta + q \sin \delta)}{R(R + \xi)}$$

$$+ \frac{q\xi}{R(R + \eta)}, \qquad \text{(A-15)}$$

and

$$T_g(\xi, \eta) = 2I_2(\xi, \eta)\cos \delta - \sin \delta \cdot \log(R + \xi), \qquad \text{(A-16)}$$

where

$$q = y \sin \delta - d \cos \delta, \quad R = \sqrt{\xi^2 + \eta^2 + q^2} \qquad \text{(A-17)}$$

and

$$I_2(\xi, \eta) = \tan^{-1}\left(\frac{R + \xi + \eta}{q}\right). \qquad \text{(A-18)}$$

REFERENCES

Andò, B., and D. Carbone, 2001, A methodology for reducing a continuously recording gravity meter for the effect of meteorological parameters: IEEE Transactions on Instrumentation and Measurements, **50**, 1248–1254.
——, 2004, A test on a neuro-fuzzy algorithm used to reduce continuous gravity records for the effect of meteorological parameters: Physics of the Earth and Planetary Interiors, **142**, 37–47.
——, 2006, A new computational approach to reduce the signal from continuously recording gravimeters for the effect of atmospheric temperature: Physics of the Earth and Planetary Interiors, **159**, 247–256.
Arnoso, J., M. Benavent, B. Ducarme, and F. G. Montesinos, 2006, A new ocean tide loading model in the Canary Islands region: Journal of Geodynamics, **41**, 100–111.
Battaglia, M., and P. Segall, 2004, The interpretation of gravity changes and crustal deformation in active volcanic areas: Pure and Applied Geophysics, **161**, 1453–1467.
Battaglia, M., P. Segall, J. Murray, P. Cervelli, and J. Langbein, 2003a, The mechanics of unrest at Long Valley caldera, California: 1. Modeling the geometry of the source using GPS, leveling and 2-color EDM data: Journal of Volcanolological and Geothermal Research, **127**, 195–217.
Battaglia, M., P. Segall, and C. Roberts, 2003b, The mechanics of unrest at Long Valley caldera, California: 2. Constraining the nature of the source using geodetic and micro-gravity data: Journal of Volcanology and Geothermal Research, **127**, 219–245.
Battaglia, M., C. Troise, F. Obrizzo, F. Pingue, and G. De Natale, 2006, Evidence for fluid migration as the source of deformation at Campi Flegrei caldera (Italy): Geophysical Research Letters, **33**, L01307, doi: 10.1029/2005GL024904.
Berrino, G., 1994, Gravity changes induced by height-mass variations at the Campi Flegrei caldera: Journal of Volcanology and Geothermal Research, **61**, 293–309.
Berrino, G., G. Corrado, G. Luongo, and B. Toro, 1984, Ground deformation and gravity changes accompanying the 1982 Pozzuoli uplift: Bulletin of Volcanology, **47**, 187–200.
Berrino, G., and U. Riccardi, 2001, Gravity tide at Mt. Vesuvius (southern Italy): Correlations with different geophysical data and volcanological implications: Journal of the Geodetic Society of Japan, **47**, 121–127.
Bonaccorso, A., S. Cianetti, C. Giunchi, E. Trasatti, M. Bonafede, and E. Boschi, 2005, Analytical and 3-D numerical modelling of Mt. Etna (Italy) volcano inflation: Geophysical Journal International, **163**, 852–862.
Bonafede, M., and M. Mazzanti, 1998, Modelling gravity variations consistent with ground deformation in the Campi Flegrei caldera (Italy): Journal of Volcanological and Geothermal Research, **81**, 137–157.
Bonvalot, S., M. Diament, and G. Gabalda, 1998, Continuous gravity recording with Scintrex CG-3M meters: A promising tool for monitoring active zones: Geophysical Journal International, **135**, 470–494.
Boy, J.-P., J. Hinderer, and P. Gegout, 1998, Global atmospheric loading and gravity: Physics of the Earth and Planetary Interiors, **109**, 161–177.
Branca, S., D. Carbone, and F. Greco, 2003, Intrusive mechanism of the 2002 NE-Rift eruption at Mt. Etna (Italy) inferred through continuous microgravity data and volcanological evidences: Geophysical Research Letters, **30**, doi: 10.1029/2003GL018250.
Budetta, G., and D. Carbone, 1997, Potential application of the Scintrex CG-3M gravimeter for monitoring volcanic activity: Results of field trials on

Mt. Etna, Sicily: Journal of Volcanology and Geothermal Research, **76**, 199–214.
Carbone, D., G. Budetta, and F. Greco, 2003a, Bulk processes some months before the start of the 2001 Mt. Etna eruption, highlighted through microgravity studies: Journal of Geophysical Research, **108**, doi: 10.1029/2003JB002542.
Carbone, D., G. Budetta, F. Greco, and H. Rymer, 2003b, Combined discrete and continuous gravity observations at Mount Etna: Journal of Volcanology and Geothermal Research, **123**, 123–135.
Carbone, D., L. Zuccarello, and G. Saccorotti, 2008, Geophysical indications of magma uprising at Mt. Etna during the December 2005 to January 2006 non-eruptive period: Geophysical Research Letters, **35**, L06305, doi: 10.1029/2008GL033212.
Carbone, D., L. Zuccarello, G. Saccorotti, and F. Greco, 2006, Analysis of simultaneous gravity and tremor anomalies observed during the 2002-2003 Etna eruption: Earth and Planetary Science Letters, **245**, 616–629.
Cayol, V., and F. Cornet, 1998, Effects of topography on the interpretation of the deformation field of prominent volcanoes: Application to Etna: Geophysical Research Letters, **25**, 1979–1982.
Charco, M., L. Brimich, and J. Fernández, 2002, Topography effects on the displacements and gravity changes due to magma intrusion: Geologica Carpathica, **53**, 215–221.
Charco, M., J. Fernández, F. Luzón, and J. B. Rundle, 2006, On the relative importance of self-gravitation and elasticity in modelling volcanic ground deformation and gravity changes: Journal of Geophysical Research, **111**, B03404, doi: 10.1029/2005JB003754.
Charco, M., J. Fernández, F. Luzón, K. F. Tiampo, and J. B. Rundle, 2007a, Some insights about topographic, elastic and self-gravitation interaction in modelling ground deformation and gravity changes in active volcanic areas: Pure and Applied Geophysics, **164**, 865–878.
Charco, M., F. Luzón, J. Fernández, and K. F. Tiampo, 2007c, Topography and self-gravitation interaction in elastic-gravitational modeling: Geochemistry, Geophysics, Geosystems (G*3*), **8**, Q01001, doi: 10.1029/2006GC001412.
Charco, M., F. Luzón, J. Fernández, K. F. Tiampo, and F. J. Sánchez-Sesma, 2007b, Three-dimensional indirect boundary element method for deformation and gravity changes in volcanic areas: Application to Teide volcano (Tenerife, Canary Islands): Journal of Geophysical Research, **112**, B08409, doi: 10.1029/2006JB004740.
Clark, D. A., S. J. Saul, and D. W. Emerson, 1986, Magnetic and gravity anomalies of a triaxial ellipsoid: Exploration Geophysics, **17**, 189–200.
Currenti, G., C. Del Negro, and G. Ganci, 2007, Modelling of ground deformation and gravity fields using finite element method: An application to Etna volcano: Geophysical Journal International, **169**, doi: 10.111/j.1365–246X.2007.03380.x.
De Meyer, F., B. Ducarme, A. Elwahabi, G. Berrino, and H. Rymer, 1995, Continuous gravity observations at Mount Etna (Sicily): Presented at the 21st General Assembly, IUGG.
De Natale, G., and F. Pingue, 1996, Ground deformation modeling in volcanic areas, *in* R. Tilling and R. Scarpa, eds., Monitoring and mitigation of volcano hazard: Springer, 385–389.
Dieterich, J. H., and R. W. Decker, 1975, Finite element modeling of surface deformation associated with volcanism: Journal of Geophysical Research, **80**, 4095–4102.
Dvorak, J. J., and D. Dzurisin, 1997, Volcano geodesy: The search for magma reservoirs and the formation of eruptive vents: Reviews of Geophysics, **35**, 343–384.
Dzurisin, D., 2003, A comprehensive approach to monitoring volcano deformation as a window on the eruptive cycle: Reviews of Geophysics, **41**, 1009, doi: 10.1029/2003RG000134.
Eggers, A. A., 1987, Residual gravity changes and eruption magnitudes: Journal of Volcanology and Geothermal Research, **33**, 201–216.
El Wahabi, A., B. Ducarme, M. Van Ruymbeke, N. d'Oreyè, and A. Somerhausen, 1997, Continuous gravity observations at Mount Etna (Sicily) and correlations between temperature and gravimetric records: Cahiers du Centre Européen de Géodynamique et de Séismologie, **14**, 105–119.
Ferguson, J. F., F. J. Klopping, T. Chen, J. E. Seibert, J. L. Hare, and J. L. Brady, 2008, The 4D microgravity method for waterflood surveillance: Part III — 4D absolute microgravity surveys at Prudhoe Bay, Alaska: Geophysics 0016-8033, **73**, this issue.
Fernández, J., M. Charco, J. B. Rundle, and K. F. Tiampo, 2006, A revision of the FORTRAN codes GRAVW to compute deformation produced by a point magma intrusion in elastic-gravitational layered earth models: Computers & Geosciences, **32**, 275–281, doi: 10.1016/j.cageo.2005.06.015.
Fernández, J., M. Charco, K. F. Tiampo, G. Jentzsch, and J. B. Rundle, 2001a, Joint interpretation of displacements and gravity data in volcanic areas: A test example: Long Valley Caldera, California: Geophysical Research Letters, **28**, 1063–1066.
Fernández, J., and J. B. Rundle, 1994, Gravity changes and deformation due to a magmatic intrusion in a two-layered crustal model: Journal of Geophysical Research, **99**, 2737–2746.
Fernández, J., J. B. Rundle, R. D. R. Granell, and T.-T. Yu, 1997, Programs to

compute deformation due to a magma intrusion in elastic-gravitational layered earth models: Computers & Geosciences, **23**, 231–249.

Fernández, J., K. F. Tiampo, G. Jentzsch, M. Charco, and J. B. Rundle, 2001b, Inflation or deflation? New results for Mayon volcano applying elastic-gravitational modeling: Geophysical Research Letters, **28**, 2349–2352.

Fernández, J., K. F. Tiampo, J. B. Rundle, and G. Jentzsch, 2005, On the interpretation of vertical gravity gradients produced by magmatic intrusions: Journal of Geodynamics, **39**, 475–492, doi: 10.1016/j.jog.2005.04.005.

Fialko, Y., Y. Khazan, and M. Simons, 2001, Deformation due to a pressurized horizontal circular crack in an elastic half-space, with applications to volcano geodesy: Geophysical Journal International, **146**, 181–190.

Folch, A., J. Fernández, J. B. Rundle, and J. Martí, 2000, Ground deformation in a viscoelastic medium composed of a layer overlying a half space: A comparison between point and extended sources: Geophysical Journal International, **140**, 37–50.

Folch, A., and J. Gottsmann, 2006, Faults and ground uplift at active calderas: *in* C. Troise, G. De Natale, and C. Kilburn, eds., Mechanisms of activity and unrest at large calderas: Special Publications, Geological Society [London], 109–120.

Furuya, M., S. Okubo, F. Kimata, R. Miyajima, I. Meilano, W. Sun, Y. Tanaka, and T. Miyazaki, 2003a, Mass budget of the magma flow in the 2000 volcano-seismic activity at Izu-islands, Japan: Earth Planets Space, **55**, 375–385.

Furuya, M., S. Okubo, W. Sun, Y. Tanaka, J. Oikawa, H. Watanabe, and T. Maekawa, 2003b, Spatiotemporal gravity changes at Miyakejima volcano: Japan: Caldera collapse, explosive eruptions and magma movement: Journal of Geophysical Research, **108**, doi: 10.1029/2002JB001989.

Gottsmann, J., and M. Battaglia, 2008, Deciphering causes of unrest at collapse calderas: Recent advances and future challenges of joint gravimetric and ground deformation studies: *in* J. Gottsmann and J. Martí, eds., Caldera volcanoes: Analysis, modeling and response: Elsevier, 417–446.

Gottsmann, J., G. Berrino, H. Rymer, and G. Williams-Jones, 2003, Hazard assessment during caldera unrest at the Campi Flegrei, Italy: A contribution from gravity-height gradients: Earth and Planetary Science Letters, **211**, 295–309.

Gottsmann, J., A. Camacho, K. F. Tiampo, and J. Fernández, 2006a, Spatiotemporal variations in vertical gravity gradients at the Campi Flegrei caldera (Italy): A case for source multiplicity during unrest?: Geophysical Journal International, **167**, 1089–1096.

Gottsmann, J., R. Carniel, N. Coppo, L. Wooller, S. Hautmann, and H. Rymer, 2007, Oscillations in hydrothermal systems as a source of periodic unrest at caldera volcanoes: Multiparameter insights from Nisyros Greece: Geophysical Research Letters, **34**, L07307, doi: 10.1029/2007GL029594.

Gottsmann, J., and H. Rymer, 2002, Deflation during caldera unrest: Constraints on subsurface processes and hazard prediction from gravity-height data: Bulletin of Volcanology, **64**, 338–348.

Gottsmann, J., H. Rymer, and L. K. Wooller, 2005, On the interpretation of gravity variations in the presence of active hydrothermal systems: Insights from the Nisyros caldera, Greece: Geophysical Research Letters, **32**, L23310, doi: 10.1029/2005GL024061.

Gottsmann, J., L. K. Wooller, J. Marti, J. Fernández, A. G. Camacho, P. Gonzalez, A. García, and H. Rymer, 2006b, New evidence for the reactivation of Teide volcano: Geophysical Research Letters, **33**, L20311, doi: 10.1029/2006GL027523.

Gudmundsson, A., 2006, How local stresses control magma-chamber ruptures, dyke injections, and eruptions in composite volcanoes: Earth-Science Review, **79**, 1–31.

Hagiwara, Y., 1978, The Mogi model as a possible cause of the crustal uplift in the eastern part of Izu Peninsula and related gravity change: Bulletin of the Earthquake Research Institute, University of Tokyo, **52**, 301–309.

Jachens, R. C., and C. W. Roberts, 1985, Temporal and areal gravity investigations at Long Valley caldera, California: Journal of Geophysical Research, **90**, 11210–11218.

Jaupart, C., and S. Vergniolle, 1988, Dynamics of degassing at Kilauea volcano, Hawaii: Nature, **311**, 58–60.

Johnsen, G. V., A. Bjornsson, and S. Sigurdsson, 1980, Gravity and elevation changes caused by magma movement beneath the Krafla caldera, northeast Iceland: Journal of Geophysics, **47**, 132–140.

Jousset, P., S. Dwipa, F. Beauducel, T. Duquesnoy, and M. Diament, 2000, Temporal gravity at Merapi during the 1993–1995 crisis: An insight into the dynamical behavior of volcanoes: Journal of Volcanological and Geothermal Research, **100**, 289–320.

Jousset, P., and H. Okada, 1999, Post-eruptive volcanic dome evolution as revealed by deformation and microgravity observations at Usu volcano (Hokkaido, Japan): Journal of Volcanology and Geothermal Research, **89**, 255–273.

LaCoste & Romberg, 2004, Instruction manual. Model G and D gravity meters: www.gravity-meta-repair.com/images/gdmanual.pdf (last accessed August, 5, 2008).

Lisowsky, M., 2006, Analytical volcano deformation source parameters, *in* D. Dzurisin, Volcano deformation: New geodetic monitoring techniques: Springer-Verlag, 441–481.

Lungarini, L., C. Troise, M. Meo, and G. De Natale, 2005, Finite element modelling of topographic effects on elastic ground deformation at Mt. Etna: Journal of Volcanology and Geothermal Research, **144**, 257–271.

Masterlark, T., 2007, Magma intrusion and deformation predictions: Sensitivities to the Mogi assumptions: Journal of Geophysical Research, **112**, B06419, doi: 10.1029/2006JB004860.

McTigue, D. F., 1987, Elastic stress and deformation near a finite spherical magma body: Resolution of the point source paradox: Journal of Geophysical Research, **92**, 12931–12940.

McTigue, D. F., and P. Segall, 1988, Displacements and tilts from dip-slip faults and magma chambers beneath irregular surface topography: Geophysical Research Letters, **15**, 601–604.

McTigue, D. F., and D. Stein, 1984, Topographic amplification of tectonic displacements: Implications for geodetic measurements of strain changes: Journal of Geophysical Research, **89**, 1123–1131.

Merriam, J. B., 1992, Atmospheric pressure and gravity: Geophysical Journal International, **109**, 488–500.

Newman, A. V., T. H. Dixon, and N. Gourmelen, 2006, A four-dimensional viscoelastic deformation model for Long Valley caldera, California, between 1995 and 2000: Journal of Volcanology and Geothermal Research, **150**, 244–269.

Okada, Y., 1985, Surface deformation due to shear and tensile faults in a half-space: Bulletin of the Seismological Society of America, **75**, 1135–1154.

Okubo, S., 1992, Gravity and potential changes due to shear and tensile faults in a half-space: Journal Geophysical Research, **97**, 7137–7144.

Okubo, S., Y. Hirata, M. Sawada, and K. Nagasawa, 1991, Gravity change caused by the 1989 earthquake swarm and submarine eruption off Ito, Japan: Test on the magmatic intrusion hypothesis: Journal of Physics of the Earth, **39**, 219–230.

Rundle, J. B., 1978, Gravity changes and the Palmdale uplift: Geophysical Research Letters, **5**, 41–44.

——, 1980, Static elastic-gravitational deformation of a layered half space by point couple sources: Journal of Geophysical Research, **85**, 5355–5363.

——, 1982, Deformation, gravity, and potential changes due to volcanic loading of the crust: Journal of Geophysical Research, **87**, 10729–10744.

Rymer, H., 1989, A contribution to precision microgravity data analysis using LaCoste and Romberg gravity meters: Geophysical Journal, **97**, 311–322.

——, 1994, Microgravity change as a precursor to volcanic activity: Journal of Volcanology and Geothermal Research, **61**, 311–328.

Rymer, H., J. B. Murray, G. C. Brown, F. Ferrucci, and J. McGuire, 1993, Mechanisms of magma eruption and emplacement at Mt. Etna between 1989 and 1992: Nature, **361**, 439–441.

Rymer, H., and G. Williams-Jones, 2000, Volcanic eruption prediction: Magma chamber physics from gravity and deformation measurements: Geophysical Research Letters, **27**, 2389–2392.

Sánchez-Sesma, F., and F. Luzón, 1995, Seismic response of three dimensional alluvial valleys for incident P, S and Rayleigh waves: Bulletin of the Seismological Society of America, **85**, 269–284.

Sparks, R. S. J., 2003, Forecasting volcanic eruptions: Earth and Planetary Science Letters, **210**, 1–15.

Tiampo, K. F., J. Fernández, G. Jentzsch, M. Charco, and J. B. Rundle, 2004, Volcanic source inversion using a genetic algorithm and an elastic-gravitational layered earth model for magmatic intrusion: Computers & Geosciences, **30**, 985–1001.

Tiampo, K. F., J. B. Rundle, J. Fernández, and J. O. Langbein, 2000, Spherical and ellipsoidal volcanic sources at Long Valley caldera, California, using a genetic algorithm inversion technique: Journal of Volcanology and Geothermal Research, **102**, 189–206.

Torge, W., 1989, Gravimetry: Walter de Gruyter.

Trasatti, E., C. Giunchi, and M. Bonafede, 2003, Effects of topography and rheological layering on ground deformation in volcanic regions: Journal of Volcanology and Geothermal Research, **122**, 89–110.

Van Dam, T., J. Wahr, and D. Lavallee, 2007, A comparison of annual vertical crustal displacements from GPS and gravity recovery and climate experiment (GRACE) over Europe: Journal of Geophysical Research, **112**, B03404, doi: 10.1029/2006JB004335.

Walsh, J. B., and J. R. Rice, 1979, Local changes in gravity resulting from deformation: Journal of Geophysical Research, **84**, 165–170.

Welch, P. D., 1967, The use of fast Fourier transform for the estimation of power spectra: A method based on time averaging over short, modified periodograms: IEEE Transactions of Audio and Electroacoustics, **15**, 70–73.

Williams, C., and G. Wadge, 1998, The effects of topography on magma chamber deformation models: Application to Mt. Etna and radar interferometry: Geophysical Research Letters, **84**, 1549–1552.

——, 2000, An accurate and efficient method for including the effects of topography in three-dimensional elastic models of ground deformation with

applications to radar interferometry: Journal of Geophysical Research, **105**, 8103–8120.

Williams-Jones, G., and H. Rymer, 2002, Detecting volcanic eruption precursors: A new method using gravity and deformation measurements: Journal of Volcanology and Geothermal Research, **113**, 379–389.

Williams-Jones, G., H. Rymer, G. Mauri, J. Gottsmann, M. Poland, and D. Carbone, 2008, Towards continuous 4D microgravity monitoring of volcanoes: Geophysics, **73**, this issue.

Yang, X., P. M. Davis, and J. H. Dieterich, 1988, Deformation from inflation of a dipping finite prolate spheroid in an elastic half-space as a model for volcanic stressing: Journal of Geophysical Research, **93**, 4249–4257.

Yu, T.-T., J. B. Rundle, and J. Fernández, 1996, Surface deformation due to a strike-slip fault in an elastic gravitational layer overlying a viscoelastic gravitational half-space: Journal of Geophysical Research, **104**, 15313–15316.